Check for updates

ChemistrySelect

Research Article
doi.org/10.1002/slct.202501424

Chemistry Europe
European Chemical Societies Publishing

www.chemistryselect.org

Development of Benzoxazole Derivatives Targeting mTOR: A Promising Approach for Breast Cancer Therapy

Mehmet Abdullah Alagoz,*[a] Meryem Temiz Resitoglu,[b] Burak Kuzu,[c] Zainab Sabrie,[b, d] Derya Yetkin,[e] Cengiz Zobi,[f] Rukiye Nalan Tiftik,[g] Seyhan Sahan Firat,[b] Sule Gursoy,[h] Ceylan Hepokur,[i] and Oztekin Algul*[f, j]

Clinical use of mTOR inhibitors in cancer treatment is well established due to the critical role of mTOR signaling in tumor progression. In this study, we report the structure-based design and biological evaluation of a series of benzoxazole derivatives as potential mTOR inhibitors. Cytotoxicity studies using MTT assays showed that compounds B4, B11, B12, and B20 exhibited significant antiproliferative effects against breast cancer cell lines with IC_{5n} values between 4.96 and 9.82 μM. Colorimetric enzymatic assays further revealed that among these, only B12 and B20 effectively inhibited mTOR phosphorylation at Ser2448 in MCF-7 cells. Additionally, both compounds modulated the expression of key apoptotic proteins, including Bax, caspase-3, p53, and Bcl2. Molecular docking studies against the 4JT5 protein demonstrated binding affinities with docking scores ranging from −7.084 to −7.426 kcal/mol, comparable to the reference compound P2X (−7.309 kcal/mol). Molecular dynamics simulations over 150 ns confirmed the stability of B12 and B20 in the active site, with an average RMSD of 2.8 Å and 3.0 Å, respectively. The absorption, distribution, metabolism, excretion, and toxicity (ADMET) properties of the synthesized compounds were evaluated in silico. Among them, B4, B11, B12, and B20 exhibited drug-like characteristics and showed no undesirable toxic effects. These findings highlight the potential of B12 and B20 as lead compounds for the development of novel mTOR inhibitors in breast cancer therapy.

[a] *M. A. Alagoz*
Department of Pharmaceutical Chemistry, Faculty of Pharmacy, Inonu University, Malatya, Türkiye
E-mail: mehmet.alagoz@inonu.edu.tr

[b] *M. T. Resitoglu, Z. Sabrie, S. S. Firat*
Department of Pharmacology, Faculty of Pharmacy, Mersin University, Mersin, Türkiye

[c] *B. Kuzu*
Department of Pharmaceutical Chemistry, Faculty of Pharmacy, Van Yüzüncü Yıl University, Van, Türkiye

[d] *Z. Sabrie*
Faculty of Medicine and Health Sciences, Simad University, Mogadishu, Somalia

[e] *D. Yetkin*
Advance Technology Education Research and Application Centre, Mersin University, Mersin, Türkiye

[f] *C. Zobi, O. Algul*
Department of Pharmaceutical Chemistry, Faculty of Pharmacy, Erzincan Binali Yıldırım University, Erzincan, Türkiye
E-mail: oztekinalgul@mersin.edu.tr

[g] *R. N. Tiftik*
Department of Pharmacology, Faculty of Medicine, Mersin University, Mersin, Türkiye

[h] *S. Gursoy*
Department of Biochemistry, Faculty of Pharmacy, Erzincan Binali Yıldırım University, Erzincan, Türkiye

[i] *C. Hepokur*
Department of Biochemistry, Faculty of Pharmacy, Sivas Cumhuriyet University, Sivas, Türkiye

[j] *O. Algul*
Department of Pharmaceutical Chemistry, Faculty of Pharmacy, Mersin University, Mersin, Türkiye

1. Introduction

The mammalian target of rapamycin (mTOR), a serine/threonine kinase, is a key component of the PI3K-AKT signaling pathway, regulating ribosomal translation of mRNAs into proteins essential for cell growth, progression, and metabolism. mTOR signaling is frequently overactivated in various cancers, particularly breast cancer, due to mutations in mTOR, increased activity of ErbB family receptors, or alterations in PI3K signaling. This hyperactivation poses a significant clinical challenge, highlighting the urgent need for innovative therapeutic strategies.

Somatic mutations, along with the loss or gain of key genes and other genetic alterations, disrupt this signaling pathway in many solid and hematologic tumors. Activation of the mTOR pathway, often in conjunction with other signaling pathways, results in profound deregulation of cell growth and survival, leading to increased competitive growth advantage, metastatic potential, angiogenesis, and therapy resistance.[1,2] Based on the current knowledge of mTOR function in cancer cells, these mTOR inhibitors could potentially inhibit tumor growth, induce cell cycle arrest, reduce angiogenesis, and enhance the effectiveness of other anticancer treatments.[3]

mTOR forms distinct protein complexes, mTORC1 and mTORC2, differentiated by their regulatory proteins, particularly Raptor (regulatory-associated protein of mTOR) in mTORC1 and Rictor (rapamycin-insensitive companion of mTOR) in mTORC2.[4,5] Both complexes act as scaffold proteins, facilitating the recruitment of regulators and substrates. Despite their structural similarities, mTORC1 and mTORC2 differ significantly in their sensitivity to rapamycin, integration of upstream signals,

© 2025 Wiley-VCH GmbH

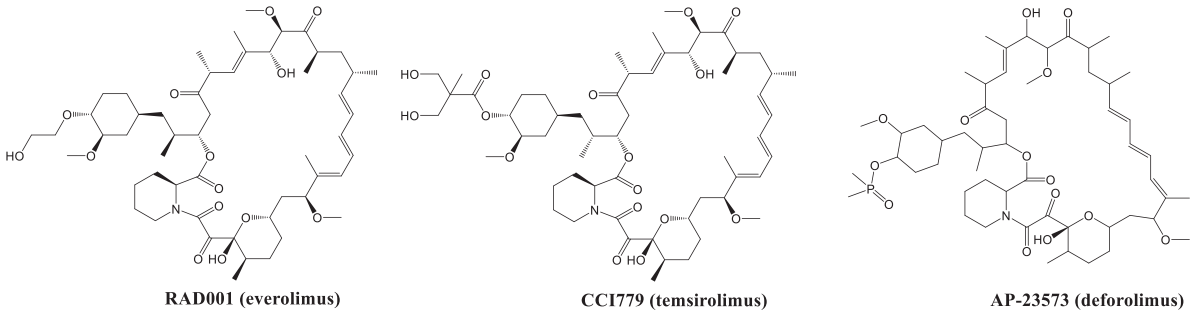

Figure 1. Rapamycin analogs (Rapaloglar).

substrates, and the biological processes they regulate. Additionally, disruptions in their activities are implicated in diverse diseases, including cancer, obesity, type 2 diabetes, neurodegenerative disorders, and inflammation.[6–8]

The mTOR inhibitors, such as rapamycin and its analogs, are being used in clinical practice to treat certain types of cancer.[9,10] Currently, only three mTOR inhibitors (rapamycin, temsirolimus, and everolimus) are clinically available in Europe. However, rapamycin's undesirable pharmacological properties necessitated the development of more reliable and effective derivatives. Among these, the rapalogs RAD001 (everolimus), CCI-779 (temsirolimus), and AP-23573 (deforolimus) demonstrated cytostatic activity in preclinical models and antitumor efficacy in combination with chemotherapies (Figure 1).[11,12]

Unlike traditional rapalogs, P2×2 (torkinib) is a pan-mTOR inhibitor capable of effectively inhibiting both mTORC1 and mTORC2 complexes, suppressing tumor growth and metastasis, particularly in cancers with hyperactive PI3K/Akt/mTOR pathways.[13–16] Its derivative INK128 (sapanisertib), along with other pan-mTOR inhibitors such as AZD-8055 and OSI-027, is in early-phase clinical trials for solid malignancies, including breast cancer. Additionally, small molecules like PKI-402, which inhibit both PI3K and mTOR pathways, have shown potent suppression of Akt phosphorylation and tumor cell growth (Figure 2).[17,18]

As an important class of compounds, benzoxazole derivatives have brought about beneficial uses in the field of pharmaceuticals.[19] Notable benzoxazole-based compounds have emerged as promising mTOR inhibitors (Figure 3). For example, K313, which reduces p-p70S6K protein levels, has demonstrated significant anticancer activity by inducing apoptosis, arresting cell cycle progression, and suppressing mTOR/p70S6K signaling pathways.[20] Similarly, eCF-309 effectively inhibits mTOR substrates, including S6K1 and 4E-BP1, demonstrating its potential for treating diseases associated with mTOR hyperactivation.[21] Developed a benzoxazole derivative with better potency against mTOR while maintaining its potent inhibitory effect against PI3K isoforms and this compound was found to exhibit excellent antiproliferative effect against a wide range of cancer cell lines and had higher potency than the related positive marketed drugs tested.[16]

Pro-inflammatory cytokines TNF-α and IL-6 can activate the mTOR signaling pathway and promote cell proliferation. Pinto et al. emphasized the regulatory role of IL-6 on mTOR activity and reported that the decrease of IL-6 caused the suppression of mTOR.[22] It was reported that rapamycin reduced mTOR activity by inhibiting TNF-α and IL-6, thus reducing inflammation. This clearly demonstrates the connection of the mTOR pathway with inflammatory signals.[23–25] There are studies indicating that benzoxazole derivatives may exhibit anti-cancer activity through mTOR inhibition. It is known that the inhibition of the PI3K/Akt/ pathway in MCF-7 cells reduces cell growth and increases apoptosis.[26] Our group has recently investigated 5-methoxy-N-phenylbenzo[d]oxazole-2-carboxamide (RBK-13) which significantly anti-inflammatory effects reduced TNF-α and IL-6 production in LPS-activated macrophages and exhibited potent antiproliferative effects in MCF-7 ($IC_{5n} = 34.7$ nM) and DU-145 ($IC_{5n} = 72.0$ nM) cancer cell lines. Notably, compounds containing a benzoxazole moiety exhibit more potent antiproliferative effects, as well as stronger mTOR and PI3K inhibitory activity, compared to those with a benzimidazole or benzisoxazole moiety. This suggests that the potency of these compounds is influenced by the presence and positioning of oxygen and nitrogen atoms.[16] Based on the above findings suggest that benzoxazole derivatives are promising scaffolds for developing potent mTOR inhibitors.

Most of the latest reported PI3K/mTOR inhibitors aiming at the treatment of colorectal cancer, breast cancer, gastric cancer, and prostate cancer, exhibited good cellular and kinase activity, but there are still some significant problems remain unsolved, such as the poor oral bioavailability and potential clinical side effects, which hinders the further clinical applications.[27–31] Therefore, the development of innovative inhibitors with good physicochemical and pharmacokinetic (PK) properties, specifically targeting the mTOR kinase for further clinical trials in the treatment of cancer, is currently insufficient.

Our laboratory has been actively involved in the research and development of benzoxazole analogues, focusing on their chemical derivatization, synthesis, and pharmacological evaluation. Based on K313, 20 benzoxazole derivatives were designed, synthesized, and evaluated for their mTOR inhibitory and anticancer activities (Figure 4). In silico studies, including molecular docking and dynamics simulations, were also conducted to elucidate their interactions with target proteins and support structure–activity relationships.

© 2025 Wiley-VCH GmbH

23656549, 2025, 21, Downloaded from https://chemistry-europe.onlinelibrary.wiley.com/doi/10.1002/slct.202501424 by Erzincan Universitesi, Wiley Online Library on [01/06/2025]. See the Terms and Conditions (https://onlinelibrary.wiley.com/terms-and-conditions) on Wiley Online Library for rules of use; OA articles are governed by the applicable Creative Commons License

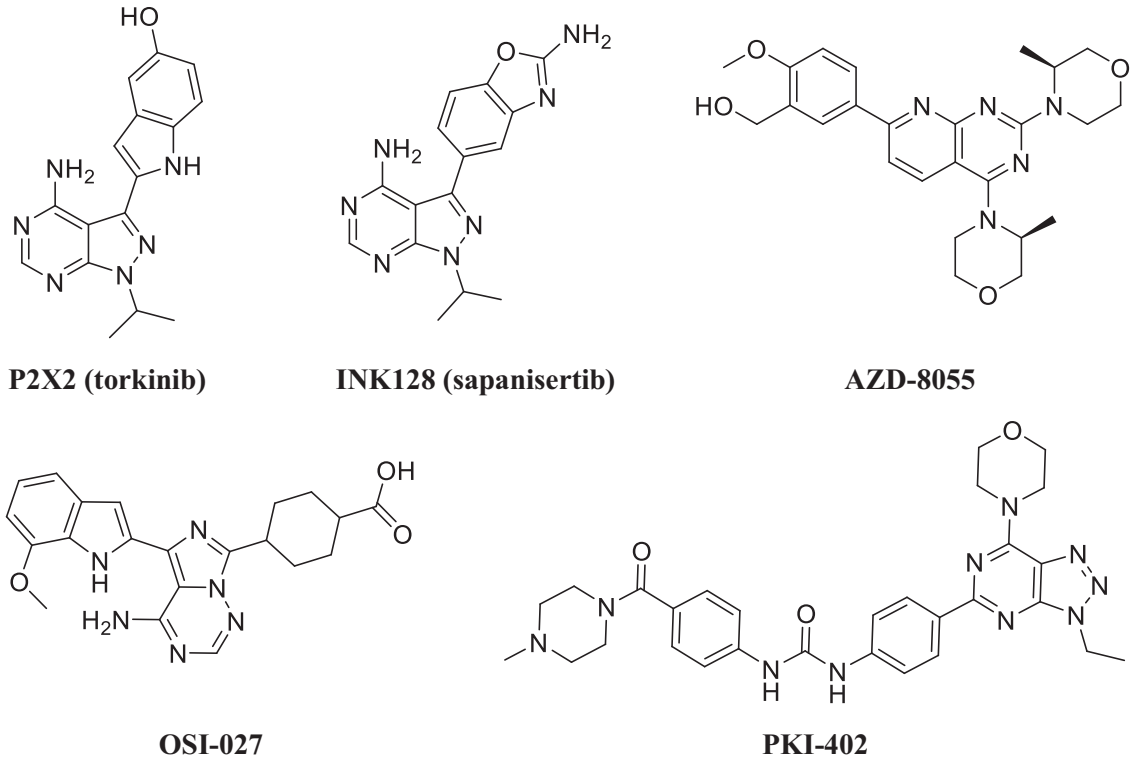

Figure 2. Key mTOR Inhibitors.

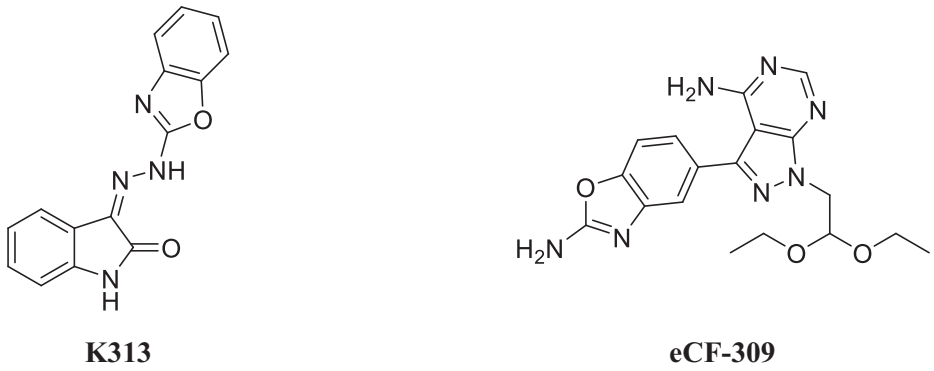

Figure 3. Benzoxazole- based mTOR inhibitor compounds.

2. Materials and Methods

2.1. Chemistry

2.1.1. General

Chemicals and all the solvents were purchased locally from Aldrich (Germany) and Acros (Germany) chemical and used without further purification unless. Melting points of the compounds were recorded on an Electrothermal-9200 digital melting points apparatus and are uncorrected. The ^{1}H-NMR and ^{13}C-NMR spectra were recorded in $CDCl_3$ on Bruker 400 MHz NMR spectrometer. Chemical shifts are reported in parts per million relatives to internal standard tetramethylsilane (TMS). Thin layer chromatography (TLC) carried out on silica gel 60 (Merck; 230–400 mesh ASTM). Elemental analysis was performed on a Leco 932 CHNS instrument (St. Joseph. MI. USA) and the results were within ±0.4% of the theoretical values.

2.1.2. General Procedure for Intermediates 7–11

Under reflux conditions, substituted 2-aminophenols (5 mmol) (1–5) in EtOH (10 mL) underwent a substitution reaction with diethyl oxalate (7.5 mmol) (6) for 6 h. The reaction was monitored by TLC until the completion of the reaction. After completion, the reaction medium was cooled to 25 °C, filtered and washed with EtOH (10 mL). The obtained solid material was dried over at 60 °C for overnight in vacuum (Scheme 1).[32–34]

© 2025 Wiley-VCH GmbH

23656549, 2025, 21, Downloaded from https://chemistry-europe.onlinelibrary.wiley.com/doi/10.1002/slct.202501424 by Erzincan Universitesi, Wiley Online Library on [01/06/2025]. See the Terms and Conditions (https://onlinelibrary.wiley.com/terms-and-conditions) on Wiley Online Library for rules of use; OA articles are governed by the applicable Creative Commons License

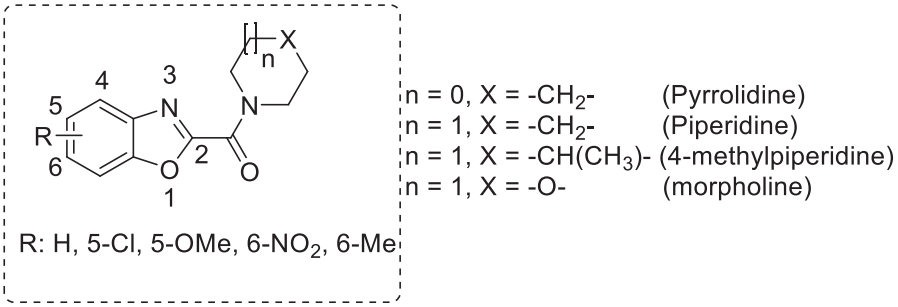

Figure 4. Designed benzoxazole derivative compounds.

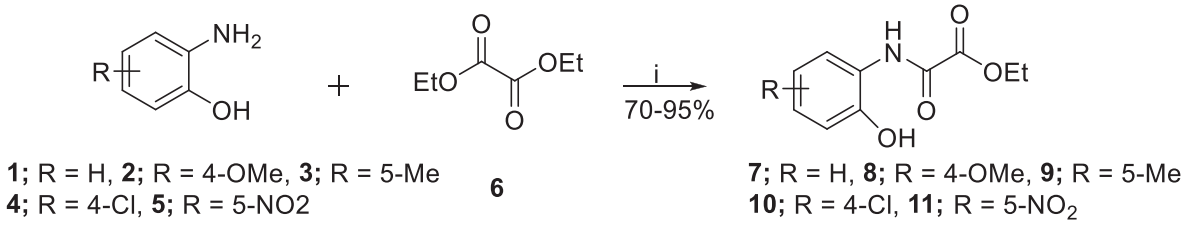

Scheme 1. General procedure for intermediates **7–11** (i); 10 mL EtOH, reflux, 6 h and 2 h.

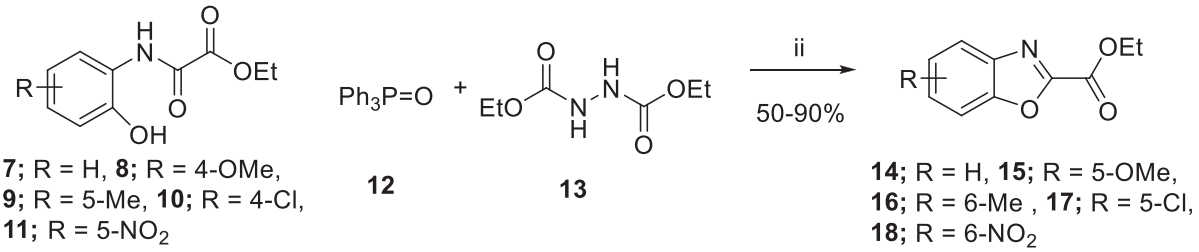

Scheme 2. General procedure for benzoxazole-2-ethyl-carboxylates (**14–18**) (ii); 1.5 equiv. DEAD, 1.3 equiv. PPh_3, 10 mL THF room temperature, and 0.5 h.

2.1.3. General Procedure for Benzoxazole-2-ethyl-carboxylates (14–18)

PPh_3 (1.3 mmol) was dissolved in THF (10 mL) and DEAD (1.5 mmol) was added dropwise to this solution. The mixture was stirred for 1 h at room temperature. After 1 h, synthesized 2-hydroxyamino-2-oxoacetate derivative (1 mmol) was dissolved in THF (10 mL) and added dropwise to the reaction mixture. The mixture was stirred at room temperature for 30 min. After completion of the reaction, monitored by TLC, solvent in the reaction medium was removed under reduced pressure. The residue was purified with column chromatography 5:1 (n-hexane: ethyl acetate) to afford pure products **14–18** (Scheme 2).[35]

2.1.4. General Procedure for Target Compounds B1–B20

Benzoxazole-2-ethyl-carboxylate (0.5 mmol) derivatives (**14–18**) were dissolved in dry THF (7 mL). Alicyclic amine (1.2 mmol) derivatives were added to reaction mixture. The reaction mixture was heated to 60 °C and stirred until the reaction was complete. After completion the reaction, the mixture was cooled to room temperature, filtered, and solvent was removed under reduced pressure. The obtained oily material was washed with diethyl ether. The crude compounds were purified with column chromatography (*n*-hexane: ethylacetate; 5:1) and washed with diethyether to afford pure products **B1–B20** (Scheme 3).[36]

(5-Chlorobenzo[d]oxazol-2-yl)(pyrrolidin-1-yl)methanone (***B1***): Recrystallized in diethyl ether; Light gray solid; yield 93%; m.p. 148–149 °C, ^{1}H NMR (400 MHz, $CDCl_3$) δ 6.87 (d, J = 2.35 Hz, 1H, Ar—H), 6.80 (dd, J = 2.35 Hz, J = 8.50 Hz, 1H, Ar—H), 6.73 (d, J = 8.50 Hz, 1H, Ar—H), 3.66–3.53 (m, AA'BB' system, 2H, —CH_2—), 3.42–3.29 (m, AA'BB' system, 2H, —CH_2—), 3.09–2.79 (m, AA'BB' system, 2H, —CH_2—), 1.96–1.88 (m, AA'BB' system, 2H, —CH_2—). ^{13}C NMR (100 MHz, $CDCl_3$) δ 154.0, 148.6, 127.6, 124.2, 123.5, 119.1, 114.1, 112.4, 46.4, 45.1, 25.5, 24.0. Anal. Calcd. for $C_{12}H_{11}ClN_2O_2$: C: 57.50; H: 4.42; N: 11.18; Found: C: 57.55; H: 4.41; N: 11.21.

(5-Chlorobenzo[d]oxazol-2-yl)(piperidin-1-yl)methanone (***B2***): Recrystallized in diethyl ether; White solid; yield 88%; m.p. 142–144 °C; ^{1}H NMR (400 MHz, $CDCl_3$) δ 7.78 (d, J = 1.56 Hz, 1H, Ar—H), 7.55 (d, J = 8.69 Hz, 1H, Ar—H), 7.42 (dd, J = 1.56 Hz, J = 8.69 Hz, 1H, Ar—H), 3.98–3.88 (m, AA'BB' system, 2H, —CH_2—), 3.82–3.72 (m, AA'BB' system, 2H, —CH_2—), 1.80–1.67 (m, AA'BB' system, 6H, —CH_2—). ^{13}C NMR (100 MHz, $CDCl_3$) δ 156.5, 155.8, 148.5, 141.3, 130.7, 127.3, 121.1, 112.3, 48.1, 44.0, 26.6, 25.6, 24.4. Anal. Calcd. for $C_{13}H_{13}ClN_2O_2$: C: 58.99; H: 4.95; N: 10.58; Found: C: 58.95; H: 4.91; N: 10.63.

© 2025 Wiley-VCH GmbH

23656549, 2025, 21, Downloaded from https://chemistry-europe.onlinelibrary.wiley.com/doi/10.1002/slct.202501424 by Erzincan Universitesi, Wiley Online Library on [01/06/2025]. See the Terms and Conditions (https://onlinelibrary.wiley.com/terms-and-conditions) on Wiley Online Library for rules of use; OA articles are governed by the applicable Creative Commons License

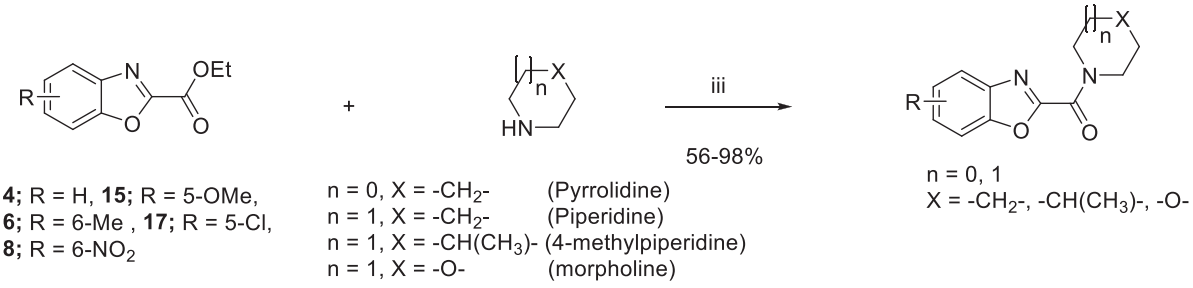

Scheme 3. General procedure for benzoxazole-2-ethyl-carboxylates (**B1–B20**) (iii); 1.2 equiv. pyrrolidine/piperidine/4-methypiperidine/morpholine in dry THF, 50–60 °C, and 0.5–2 h.

(5-Chlorobenzo[d]oxazol-2-yl)(4-methylpiperidin-1-yl)methanone (***B3***): Recrystallized in diethyl ether; White solid; yield 79%; m.p. 126–128 °C; ^{1}H NMR (400 MHz, $CDCl_3$) δ 7.76 (d, J = 2.08 Hz, 1H, Ar—H), 7.52 (d, J = 8.74 Hz, 1H, Ar—H), 7.39 (dd, J = 2.08 Hz, J = 8.74 Hz, 1H, Ar—H), 4.71–4.62 (m, AA'BB' system, 2H, —CH_2—), 3.22 (m, AA'BB' system, 1H, —CH_2—), 2.87–2.79 (m, AA'BB' system, 1H, —CH_2—), 1.81–1.72 (m, AA'BB' system, 2H, —CH_2—), 1.70–1.65 (m, 1H, —CH—), 1.33–1.25 (m, AA'BB' system, 2H, —CH_2—), 0.97 (d, J = 6.42 Hz, 3H, —CH_3). ^{13}C NMR (100 MHz, $CDCl_3$) δ 156.5, 155.8, 148.5, 141.2, 130.6, 127.3, 121.0, 112.2, 47.3, 43.4, 34.7, 33.7, 31.0, 21.6. Anal. Calcd. for $C_{14}H_{15}ClN_2O_2$: C: 60.33; H: 5.42; N: 10.05; Found: C: 60.36; H: 5.46; N: 10.01.

(5-Chlorobenzo[d]oxazol-2-yl)(morpholino)methanone (***B4***): Recrystallized in diethyl ether; White crystal solid; yield 65%; m.p.181–182 °C; ^{1}H NMR (400 MHz, $CDCl_3$) δ 7.78 (d, J = 2.04 Hz, 1H, Ar—H), 7.57 (d, J = 8.74 Hz, 1H, Ar—H), 7.45 (dd, J = 2.04 Hz, J = 8.74 Hz, 1H, Ar—H), 4.24–4.22 (m, AA'BB' system, 2H, —CH_2—), 3.87–3.79 (m, AA'BB' system, 6H, —CH_2—). ^{13}C NMR (100 MHz, $CDCl_3$) δ 155.7, 155.5, 148.5, 130.9, 127.8, 121.2, 112.4, 67.0, 66.7, 47.5, 43.3. Anal. Calcd. for $C_{12}H_{11}ClN_2O_3$: C: 54.05; H: 4.16; N: 10.50; Found: C: 54.03; H: 4.12; N: 10.52.

Benzo[d]oxazol-2-yl(pyrrolidin-1-yl)methanone (***B5***): Recrystallized in diethyl ether; Yellow solid; yield 71%; m.p. 70–72 °C; ^{1}H NMR (400 MHz, $CDCl_3$) δ 7.81 (d, J = 8.22 Hz, 1H, Ar—H), 7.64 (d, J = 8.22 Hz, 1H, Ar—H), 7.48–7.38 (m, 2H, Ar—H), 4.12 (t, J = 6.58 Hz, 2H), 3.74 (t, J = 6.58 Hz, 2H), 2.07–1.93 (m, 4H). ^{13}C NMR (100 MHz, $CDCl_3$) δ 155.8, 155.3, 150.0, 140.6, 127.1, 125.1, 121.4, 111.6, 49.3, 47.5, 29.7, 26.4, 23.9. Anal. Calcd. for $C_{12}H_{12}N_2O_2$: C: 66.65; H: 5.59; N: 12.56; Found: C: 66.73; H: 5.51; N: 12.61.

Benzo[d]oxazol-2-yl(piperidin-1-yl)methanone (***B6***): Recrystallized in diethyl ether; Brown viscous liquid; yield: 74%; ^{1}H NMR (400 MHz, $CDCl_3$) δ 7.81 (ddd, J = 0.72 Hz, J = 1.42 Hz, J = 7.55 Hz, 1H, Ar—H), 7.63 (ddd, J = 0.72 Hz, J = 1.42 Hz, J = 8.13 Hz, 1H, Ar—H), 7.45 (ddd, J = 1.42 Hz, J = 7.55 Hz, J = 8.13 Hz, 1H, Ar—H), 7.43–7.38 (m, 1H, Ar—H), 3.99–3.96 (m, 2H), 3.80–3.77 (m, 2H), 1.75–1.69 (m, 6H). ^{13}C NMR (100 MHz, $CDCl_3$) δ 156.3, 155.3, 149.9, 140.2, 126.8, 125.1, 121.2, 111.5, 48.1, 44.0, 29.7, 26.4, 26.6, 24.5. Anal. Calcd. for $C_{13}H_{14}N_2O_2$: C: 67.81; H: 6.13; N: 12.17; Found: C: 67.79; H: 6.09; N: 12.13.

Benzo[d]oxazol-2-yl(4-methylpiperidin-1-yl)methanone (***B7***): Recrystallized in diethyl ether; Light yellow solid; yield 85%; m.p. 89–90 °C; ^{1}H NMR (400 MHz, $CDCl_3$) δ 7.80 (ddd, J = 0.71 Hz, J = 1.40 Hz, J = 7.92 Hz, 1H, Ar—H), 7.62 (ddd, J = 0.71 Hz, J = 1.40 Hz, J = 7.92 Hz, 1H, Ar—H), 7.46–7.42 (m, 1H, Ar—H), 7.41–7.37 (m, 1H, Ar—H), 4.75–4.67 (m, AA'BB' system, 2H, —CH_2—), 3.25–3.18 (m, AA'BB' system, 1H, —CH_2—), 2.89–2.82 (m, AA'BB' system, 1H, —CH_2—), 1.83–1.70 (m, AA'BB' system, 3H, —CH_2—), 1.33–1.29 (m, AA'BB' system, 1H, —CH_2—), 0.99 (d, J = 6.40 Hz, 3H, —CH_3), 0.87–0.82 (m, AA'BB' system, 1H, —CH_2—). ^{13}C NMR (100 MHz, $CDCl_3$) δ 156.3, 155.4, 149.9, 140.2, 126.8, 125.1, 121.2, 111.4, 47.3, 43.3, 34.8, 33.7, 31.0, 21.5. Anal. Calcd. for $C_{14}H_{16}N_2O_2$: C: 68.83; H: 6.60; N: 11.47; Found: C: 68.82; H: 6.58; N: 11.51.

Benzo[d]oxazol-2-yl(morpholino)methanone (***B8***): Recrystallized in diethyl ether; Gray solid; yield 86%; m.p. 85–88 °C; ^{1}H NMR (400 MHz, $CDCl_3$) δ 7.81 (ddd, J = 0.67 Hz, J = 1.25 Hz, J = 7.79 Hz, 1H, Ar—H), 7.66 (ddd, J = 0.67 Hz, J = 1.25 Hz, J = 7.79 Hz, 1H, Ar—H), 7.50–7.46 (m, 1H), Ar—H), 7.44–7.40 (m, 1H, Ar—H), 4.28–4.26 (m, 2H), 3.89–3.79 (m, 6H). ^{13}C NMR (100 MHz, $CDCl_3$) δ 156.0, 149.9, 140.1, 127.3, 125.4, 121.3, 111.6, 67.1, 66.7, 47.5, 43.3. Anal. Calcd. for $C_{12}H_{12}N_2O_3$: C: 62.06; H: 5.21; N: 12.06; Found: C: 62.11; H: 5.25; N: 12.11.

(5-Methoxybenzo[d]oxazol-2-yl)(pyrrolidin-1-yl)methanone (***B9***): Recrystallized in diethyl ether; White solid; yield 98%; m.p. 166–167 °C; ^{1}H NMR (400 MHz, $CDCl_3$) δ 7.52 (d, J = 8.99 Hz, 1H, Ar—H), 7.25 (d, J = 2.50 Hz, 1H, Ar—H), 7.06 (dd, J = 2.50 Hz, J = 8.99 Hz, 1H, Ar—H), 4.13–4.09 (m, AA'BB' system, 2H, —CH_2—), 3.86 (s, 3H, OMe), 3.75–3.72 (m, AA'BB' system, 2H, —CH_2—), 2.07–1.92 (m, AA'BB' system, 4H, —CH_2—). ^{13}C NMR (100 MHz, $CDCl_3$) δ 157.7, 156.4, 155.2, 144.7, 141.4, 116.6, 111.9, 103.2, 55.9, 49.3, 47.5, 26.5, 23.9. Anal. Calcd. for $C_{13}H_{14}N_2O_3$: C: 63.40; H: 5.73; N: 11.38; Found: C: 63.38; H: 5.75; N: 11.41.

(5-Methoxybenzo[d]oxazol-2-yl)(piperidin-1-yl)methanone (***B10***): Recrystallized in diethyl ether; Grey viscous liquid; yield 69%; ^{1}H NMR (400 MHz, $CDCl_3$) δ 7.50 (d, J = 8.98 Hz, 1H, Ar—H), 7.25 (d, J = 2.54 Hz, 1H, Ar—H), 7.05 (dd, J = 2.54 Hz, J = 8.98 Hz, 1H, Ar—H), 4.00–3.95 (m, AA'BB' system, 2H, —CH_2—), 3.86 (s, 3H, OMe), 3.80–3.75 (m, AA'BB' system, 2H, —CH_2—), 1.76–1.67 (m, AA'BB' system, 4H, —CH_2—), 1.10 (bs, 1H, —CH_2—), 0.91–0.86 (m, AA'BB' system, 1H, —CH_2—). ^{13}C NMR (100 MHz, $CDCl_3$) δ 157.8, 156.3, 156.0, 144.6, 141.0, 116.2, 111.7, 103.2, 55.9, 48.0, 44.0, 26.7, 25.6, 24.5. Anal. Calcd. for $C_{14}H_{16}N_2O_3$: C: 64.60; H: 6.20; N: 10.76; Found: C: 64.56; H: 6.17; N: 10.74.

(5-Methoxybenzo[d]oxazol-2-yl)(4-methylpiperidin-1-yl)methanone (***B11***): Recrystallized in diethyl ether; Gray viscous liquid; yield 80%; ^{1}H NMR (400 MHz, $CDCl_3$) δ 7.48 (d, J = 8.99 Hz, 1H, Ar—H), 7.23 (d, J = 2.56 Hz, 1H, Ar—H), 7.03 (dd, J = 2.56 Hz, J = 8.99 Hz, 1H, Ar—H), 4.76–4.67 (m, AA'BB' system, 2H, —CH_2—), 3.84 (s, 3H, —OMe), 3.23–3.15 (m, AA'BB' system, 1H, —CH_2—),

© 2025 Wiley-VCH GmbH

23656549, 2025, 21, Downloaded from https://chemistry-europe.onlinelibrary.wiley.com/doi/10.1002/slct.202501424 by Erzincan Universitesi, Wiley Online Library on [01/06/2025]. See the Terms and Conditions (https://onlinelibrary.wiley.com/terms-and-conditions) on Wiley Online Library for rules of use; OA articles are governed by the applicable Creative Commons License

2.86–2.80 (m, AA'BB' system, 1H, —CH_2—), 1.82–1.73 (m, AA'BB' system, 2H, —CH_2—), 1.72–1.65 (m, 1H, —CH—), 1.31–1.27 (m, AA'BB' system, 1H, —CH_2—), 0.97 (d, J = 6.37 Hz, 3H, —CH_3), 0.90–0.85 (m, AA'BB' system, 1H, —CH_2—). ^{13}C NMR (100 MHz, $CDCl_3$) δ 157.8, 156.3, 156.1, 144.7, 141.1, 116.2, 111.7, 103.3, 56.0, 47.3, 43.4, 34.8, 33.8, 31.1, 21.6. Anal. Calcd. for $C_{15}H_{18}N_2O_3$: C: 65.68; H: 6.61; N: 10.21; Found: C: 65.71; H: 6.58; N: 10.20.

5-Methoxybenzo[d]oxazol-2-yl)(morpholino)methanone (***B12***): Recrystallized in diethyl ether; White solid; yield 81%; m.p. 118–120 °C, ^{1}H NMR (400 MHz, $CDCl_3$) δ 7.52 (d, J = 9.01 Hz, 1H, Ar—H), 7.23 (d, J = 2.54 Hz, 1H, Ar—H), 7.07 (dd, J = 2.54 Hz, J = 9.01 Hz, 1H, Ar—H), 4.28–4.25 (m, AA'BB' system, 2H, —CH_2—), 3.86 (s, 3H, OMe), 3.84–3.78 (m, AA'BB' system, 6H, —CH_2—). ^{13}C NMR (100 MHz, $CDCl_3$) δ 157.9, 156.0, 155.2, 144.6, 140.9, 116.8, 111.8, 103.1, 67.1, 66.7, 55.9, 47.5, 43.3. Anal. Calcd. for $C_{13}H_{14}N_2O_4$: C: 59.54; H: 5.38; N: 10.68; Found: C: 59.60; H: 5.41; N: 10.71.

(6-Methylbenzo[d]oxazol-2-yl)(pyrrolidin-1-yl)methanone (***B13***): Recrystallized in diethyl ether; Gray solid; yield 97%; m.p. 109–110 °C; ^{1}H NMR (400 MHz, $CDCl_3$) δ 7.65 (d, J = 8.23 Hz, 1H, Ar—H), 7.41 (dt, J = 0.66 Hz, J = 1.52 Hz, 1H, Ar—H), 7.19 (ddd, J = 0.66 Hz, J = 1.52 Hz, J = 8.23 Hz, 1H, Ar—H), 4.10 (t, J = 6.77 Hz, 2H, —CH_2—), 3.72 (t, J = 6.92 Hz, 1H, —CH_2—), 2.49 (s, 3H, —CH_3), 2.05–1.98 (m, 2H, —CH_2—), 1.97–1.90 (m, 2H, —CH_2—). ^{13}C NMR (100 MHz, $CDCl_3$) δ 155.4, 155.3, 150.3, 138.4, 137.9, 126.5, 120.6, 111.5, 49.2, 47.4, 26.4, 23.8, 21.9. Anal. Calcd. for $C_{13}H_{14}N_2O_2$: C: 67.81; H: 6.13; N: 12.17; Found: C: 67.85; H: 6.18; N: 12.19.

(6-Methylbenzo[d]oxazol-2-yl)(piperidin-1-yl)methanone (***B14***): Recrystallized in diethyl ether; Light Brown solid; yield 78%; m.p: 62–64 °C; ^{1}H NMR (400 MHz, $CDCl_3$) δ 7.67–7.65 (m, 1H, Ar—H), 7.41–7.40 (m, 1H, Ar—H), 7.21 (ddd, J = 0.58 Hz, J = 1.53 Hz, J = 8.21 Hz, 1H, Ar—H), 3.99–3.97 (m, AA'BB' system, 2H, —CH_2—), 3.78–3.76 (m, AA'BB' system, 2H, —CH_2—), 2.50 (s, 3H, —CH_3), 1.74–1.65 (m, AA'BB' system, 6H, —CH_2—). ^{13}C NMR (100 MHz, $CDCl_3$) δ 156.4, 154.9, 150.2, 138.0, 137.6, 126.5, 120.5, 111.4, 48.0, 44.0, 29.7, 26.7, 25.6, 24.5, 21.9. Anal. Calcd. for $C_{14}H_{16}N_2O_2$: C: 68.83; H: 6.60; N: 11.47; Found: C: 68.81; H: 6.58; N: 11.52.

(6-Methylbenzo[d]oxazol-2-yl)(4-methylpiperidin-1-yl)methanone (***B15***): Recrystallized in diethyl ether; Dark brown viscous liquid; yield 89%; ^{1}H NMR (400 MHz, $CDCl_3$) δ 7.66 (d, J = 8.20 Hz, 1H, Ar—H), 7.42–7.41 (m, 1H, Ar—H), 7.23–7.20 (m, 1H, Ar—H), 4.79–4.69 (m, AA'BB' system, 2H, —CH_2—), 3.24–3.17 (m, AA'BB' system, 1H), 2.85 (m, 1H), 2.51 (s, 3H, —CH_3), 1.83–1.70 (m, AA'BB' system, 4H, —CH_2—), 0.99 (d, J = 6.41 Hz, 3H, —CH_3), 0.89–0.85 (m, 1H). ^{13}C NMR (100 MHz, $CDCl_3$) δ 156.4, 154.9, 150.2, 138.0, 137.6, 126.5, 120.5, 111.4, 47.3, 43.3, 34.8, 33.7, 31.1, 29.7, 21.9, 21.6. Anal. Calcd. for $C_{15}H_{18}N_2O_2$: C: 69.74; H: 7.02; N: 10.84; Found: C: 69.71; H: 6.98; N: 10.79.

(6-Methylbenzo[d]oxazol-2-yl)(morpholino)methanone (***B16***): Recrystallized in diethyl ether; Brown solid; yield 86%; m.p. 93–94 °C; ^{1}H NMR (400 MHz, $CDCl_3$) δ 7.65 (d, J = 8.22 Hz, 1H, Ar—H), 7.42 (dt, J = 0.66 Hz, J = 1.48 Hz, 1H, Ar—H), 7.22 (ddd, J = 0.66 Hz, J = 1.48 Hz, J = 8.22 Hz, 1H, Ar—H), 4.28–4.25 (m, AA'BB' system, 2H, —CH_2—), 3.86–3.84 (m, AA'BB' system, 2H, —CH_2—), 3.81–3.77 (m, AA'BB' system, 4H, —CH_2—), 2.51 (s, 3H, —CH_3). ^{13}C NMR (100 MHz, $CDCl_3$) δ 156.1, 154.1, 150.2, 138.1, 137.9, 126.8, 120.6, 111.5, 67.1, 66.7, 47.5, 43.3, 21.9. Anal. Calcd. for $C_{13}H_{14}N_2O_3$: C: 63.40; H: 5.73; N: 11.38; Found: C: 63.36; H: 5.77; N: 11.41.

(6-Nitrobenzo[d]oxazol-2-yl)(pyrrolidin-1-yl)methanone (***B17***): Recrystallized in diethyl ether; Dark yellow solid; yield 56%; m.p. 174–175 °C; ^{1}H NMR (400 MHz, $CDCl_3$) δ 7.70 (d, J = 2.61 Hz, 1H, Ar—H), 7.63 (dd, J = 2.61 Hz, J = 8.75 Hz, 1H, Ar—H), 6.97 (d, J = 8.75 Hz, 1H, Ar—H), 3.74–3.46 (m, AA'BB' system, 4H, —CH_2—), 2.01 (bs, AA'BB' system, 4H, —CH_2—). ^{13}C NMR (100 MHz, $CDCl_3$) δ 162.1, 154.6, 149.6, 143.2, 141.7, 117.9, 116.1, 108.3, 47.6, 47.0, 46.5, 45.1, 25.6, 25.5, 24.3, 24.0. Anal. Calcd. for $C_{12}H_{11}N_3O_4$: C: 55.17; H: 4.24; N: 16.09; Found: C: 55.13; H: 4.29; N: 16.06.

(6-Nitrobenzo[d]oxazol-2-yl)(piperidin-1-yl)methanone (***B18***): Recrystallized in diethyl ether; Pale yellow solid; yield 97%; m.p. 210–211 °C; ^{1}H NMR (400 MHz, $CDCl_3$) δ 7.67 (d, J = 2.61 Hz, 1H, Ar—H), 7.61 (dd, J = 2.61 Hz, J = 8.75 Hz, 1H, Ar—H), 6.99 (d, J = 8.75 Hz, 1H, Ar—H), 3.86–3.66 (m, AA'BB' system, 2H, —CH_2—), 3.42–3.31 (m, AA'BB' system, 2H, —CH_2—), 3.07–2.90 (m, AA'BB' system, 2H, —CH_2—), 1.76–1.62 (m, AA'BB' system, 2H, —CH_2—), 1.45–1.35 (m, AA'BB' system, 2H, —CH_2—). ^{13}C NMR (100 MHz, $CDCl_3$) δ 161.5, 155.3, 149.7, 141.9, 118.6, 116.1, 108.3, 46.8, 41.8, 25.9, 25.1, 24.4, 23.9. Anal. Calcd. for $C_{13}H_{13}N_3O_4$: C: 56.72; H: 4.76; N: 15.27; Found: C: 56.73; H: 4.81; N: 15.23.

(4-Methylpiperidin-1-yl)(6-nitrobenzo[d]oxazol-2-yl)methanone (***B19***): Recrystallized in diethyl ether; Dark yellow solid; yield 92%; m.p. 168–169 °C; ^{1}H NMR (400 MHz, $CDCl_3$) δ 7.65–7.56 (m, 2H, Ar—H), 7.05–6.87 (m, 1H, Ar—H), 4.69–4.60 (m, AA'BB' system, 1H), 4.39–4.26 (m, AA'BB' system, 1H), 3.61–3.22 (m, AA'BB' system, 2H), 3.00–2.76 (m, AA'BB' system, 2H), 2.52–2.38 (m, AA'BB' system, 1H), 1.36–1.26 (m, 1H), 0.93–0.92 (m, 3H), 0.56 (d, J = 6.27 Hz, 1H). ^{13}C NMR (100 MHz, $CDCl_3$) δ 156.0, 149.9, 145.1, 118.9, 118.4, 116.2, 116.0, 108.2, 47.4, 45.6, 34.7, 33.6, 30.6, 21.4. Anal. Calcd. for $C_{14}H_{15}N_3O_4$: C: 58.13; H: 5.23; N: 14.53; Found: C: 58.09; H: 5.21; N: 14.49.

Morpholino(6-nitrobenzo[d]oxazol-2-yl)methanone (***B20***): Recrystallized in diethyl ether; Yellow solid; yield 71%; 170–172 °C; ^{1}H NMR (400 MHz, $CDCl_3$) δ 7.60–7.57 (m, 1H, Ar—H), 7.55 (d, J = 2.61 Hz, 1H, Ar—H), 8.61 (d, J = 8.61 Hz, 1H, Ar—H), 3.70–3.59 (m, AA'BB' system, 4H, —CH_2—), 3.54–3.50 (m, AA'BB' system, 2H, —CH_2—), 3.02–2.88 (m, AA'BB' system, 2H, —CH_2—). ^{13}C NMR (100 MHz, $CDCl_3$) δ 160.8, 154.0, 150.6, 144.5, 142.9, 121.5, 115.5, 109.5, 66.4, 66.1, 45.9, 41.1. Anal. Calcd. for $C_{12}H_{11}N_3O_5$: C: 51.99; H: 4.00; N: 15.16; Found: C: 51.95; H: 4.07; N: 15.14.

2.2. Biological Activity Studies

2.2.1. Cell Culture and MTT

Estrogen receptor positive MCF-7 human breast cancer cells (MCF-7) were cultured in RPMI-1640 medium (Gibco, USA) supplemented with 10% FBS, 100 U/mL penicillin and 100 µg/mL streptomycin at 37 °C and 5% CO_2. A standard MTT assay was used to determine the cytotoxic activity of the 20 synthesized chemicals on breast cancer. Briefly, cells were seeded in 96-well plates at a density of 3×10^4 cells per well in $n = 3$ replicates and cultured for 24 h. Cell counts and viability rates were determined using a Cedex XS device (Roche, Mannheim, Germany). The cell suspension was mixed and added to the special smart slides slide of the device and measurements were performed through the device software. Cells were then cultured at various

© 2025 Wiley-VCH GmbH

23656549, 2025, 21, Downloaded from https://chemistry-europe.onlinelibrary.wiley.com/doi/10.1002/slct.202501424 by Erzincan Universitesi, Wiley Online Library on [01/06/2025]. See the Terms and Conditions (https://onlinelibrary.wiley.com/terms-and-conditions) on Wiley Online Library for rules of use; OA articles are governed by the applicable Creative Commons License

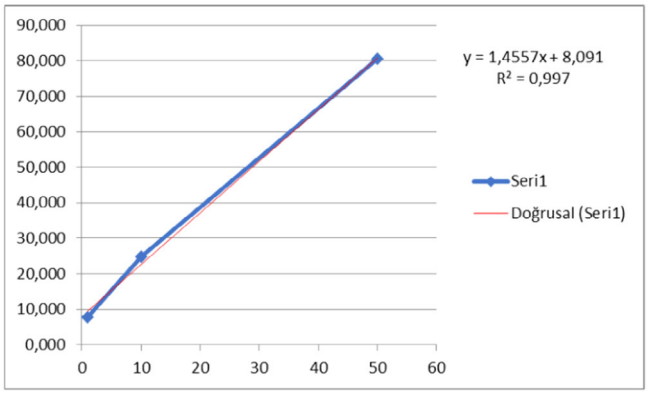

Figure 5. The absorbance value was determined in proportion to the determination of their metabolic activity with the help of Microsoft Excel programme by determining the applied dose and % cell viability curve, and the 50% suppressive concentration (IC_{50}) value logarithmic slope graph.

doses (1 μM, 10 μM, and 50 μM) for 20 synthesized chemicals, 48 and 72 h. The plates were then incubated for a further 4 h after the addition of MTT in MCF-7 cells in MCF-7 cells. To test cell viability, 100 μL DMSO was added to each well after the medium was removed and the absorbance at 570 nm was measured with a microplate reader (μQuant, BioTek Instruments, Vermont, USA). The discoloration of the formazone salts colored yellow is due to the reduction of the tetrazolium salt in the active cell mitochondria. The absorbance value of these compounds was proportional to the determination of their metabolic activity and the 50% suppressive concentration (IC_{50}) value was calculated by logarithmic slope graph by determining the applied dose and % cell viability curve with the help of Microsoft Excel programme (Figure 5).[37]

2.2.2. mTOR Activity

Chemical and reagent: The human MCF-7 cell line (HTB-22) was purchased from American Type Culture Collection (ATCC, USA). Dulbecco's modified Eagle's medium (DMEM), and penicillin–streptomycin were obtained from Gibco (New York, NY, USA). Fetal bovine serum (FBS) and trypsin-EDTA were purchased from Biological Industries (Israel). Primary antibodies for Bax (SC-23959), caspase3 (SC-56053), p53 (SC-126), Bcl2 (SC-7382), and β-actin (SC-47778) were purchased from Santa Cruz Biotechnology (Texas, USA). Additionally, secondary antibodies (goat anti-mouse IgG-horseradish peroxidase (HRP) (ab6808) and goat anti-rabbit IgG-HRP (ab6721)) were purchased from Abcam (Cambridge, United Kingdom).

Experimental groups: The cell culture was performed in DMEM/F12 containing 10% FBS, 1% penicillin-streptomycin, and L-glutamine at 37 °C in 5% CO_2 incubator. When cell confluence reached 80%, the subculture was carried out. In 6-well plates, experimental cells were cultured at a density of 2×10^4 cells per well and grown to 80%–90% confluence. Cells were divided into six groups: control; Rapa (20 μM); B4 (10,84 μM) B11 (6,40 μM); B12 (6,82 μM); and B20 (11,57 μM). All cells were incubated for 48 h at 37 °C in a 95% air, 5% CO_2 environment.

Immunoblot assay: Human MCF-7 cells (80% confluent) were quickly washed with ice-cold phosphate-buffered saline (PBS), and cells were lysed with RIPA buffer, including 1% protease and phosphatase inhibitors. Following 15 min of centrifugation at 14,000 rpm, whole-cell lysates were produced. The protein content was then assessed using the Bradford assay. Equal amounts of protein were loaded into wells, separated by electrophoresis on 10%–12% polyacrylamide–sodium dodecyl sulfate gel, and transferred to a nitrocellulose membranes. Thereafter, the membranes were blocked for 1 h at room temperature using Tris-buffered solution containing 0.05% Tween-20 (TBST) reinforced with 5% nonfat dry milk solution. Following that, the membranes were probed with specific antibodies raised against Bax, caspase3, p53, Bcl2, and β-actin (1:500–1:5000 dilutions) in TBST, including 5% BSA overnight at 4 °C. After rinsing with TBST, the membranes were incubated for 2 h at room temperature with the proper horseradish peroxidase conjugated secondary antibodies (1:1000). β-actin was used as a housekeeping protein to normalize the expression of proteins. Finally, the membranes were assayed with an enhanced chemiluminescence detection kit (ECL Plus, Western Blotting Detection Reagents) and visualized by the detection system. Densitometric analysis was performed with Image J 1.46r software (National Institutes of Health, USA).

Measurement of mTOR activity: mTOR activity in cultured screening for the effects of various treatments cells were measured by colorimetric cell-based enzyme-linked immunosorbent assay (ELISA) method as specified in the prospectus using the appropriate kit based on the principle of measuring phosphorylation of mTOR at Ser2448 as an indicator of mTORC1-mediated mTOR activity.

Statistical analysis: Data were expressed as mean ±SEM and analyzed by one-way ANOVA followed by the Newman–Keuls multiple comparison test and unpaired t test when appropriate. A p value of <0.05 was considered statistically significant. The statistical analysis was performed with GraphPad Prism (Prism 5.0; GraphPad Software, San Diego, California, USA).

2.3. In Silico Studies

2.3.1. Molecular Docking

In this study, the crystal structure of the mTOR (mechanistic target of rapamycin) enzyme was used as the target macromolecule. All modeling studies were performed using the Maestro (Schrödinger 12.8, LLC, NY) program. The crystal structure of the protein with PDB ID 4JT5 was retrieved from the Protein Data Bank and used as a reference for molecular modeling studies. For mTOR inhibition studies, the crystal structure of the relevant protein was downloaded from the RCSB Protein Data Bank (www.rcsb.org). This crystal structure was prepared using Maestro's Protein Preparation Wizard panel. Unwanted solvent

© 2025 Wiley-VCH GmbH

23656549, 2025, 21, Downloaded from https://chemistry-europe.onlinelibrary.wiley.com/doi/10.1002/slct.202501424 by Erzincan Universitesi, Wiley Online Library on [01/06/2025]. See the Terms and Conditions (https://onlinelibrary.wiley.com/terms-and-conditions) on Wiley Online Library for rules of use; OA articles are governed by the applicable Creative Commons License

molecules and ligand in the crystal structure were deleted, and hydrogens were added with Prime, Impact, Epik, and Propka software. The P2X, native ligand in the crystal, was taken in the Grid Box creation and the active sites of the 4JT5 were determined, and grid map was created.[23,38] Ligands were drawn with the 2D Sketcher interface of the program and made suitable for modeling with the LigPrep module. OPLS_2005 force field was used to optimize the structure, and energy minimization was carried out. Molecular docking operations were performed in single precision (SP) mode using the glide module, and 100 docking calculations were performed for each ligand. Docking scores are reported in kcal/mol.[38,39]

2.3.2. Molecular Dynamics Simulation Studies

Molecular dynamics simulation studies were performed using Desmond (Schrodinger 12.8). As a result of the previously performed docking studies, the pose with the highest docking score was selected for simulation. Protein–ligand complexes were placed in a 10 Å thick cubic box. The TIP3P water model was used in the simulation box.[40] The system was neutralized using Na^+ and Cl^- ions. The concentration of the system was adjusted with a 0.15 M NaCl solution. Desmod's default relaxation protocol was applied to the simulation system. The Nose–Hoover thermostat was used to regulate the systems' temperature during MD simulations, and it was initially set to 300 K. With isotropic pressure coupling, the Martyna–Tobias–Klein method was used to regulate pressure around 1.01325 bar. 9 Å cutoff for the short-range nonbonded interactions was used combined with the particle mesh Ewald option.[40,41]

2.3.3. ADMET Analysis

2D structures of compounds were drawn with the 2D Sketcher module of the Maestro (Schrodinger, 12.8.117) program and prepared with LigPrep software. The LogP, QPPCaco, QPlogBB, PSA, #metab, QPlogKhsa, % human oral absorption, and QPlogHERG properties, along with compliance to the Rule of Five and Rule of Three, were determined using QikProp (Maestro)[42] The inhibition of CYP450 and the drug-likeness characteristics of compounds, including the Veber, Egan, Ghose, and Muegge metrics, were assessed using the SwissADME online software (http://www.swissadme.ch/). Mutagenic, tumorigenic, effective, and irritant toxicological properties were assessed using DataWarrior (5.0)[41,42]

3. Results and Discussion

3.1. Chemistry

A series of novel 5/6-substituted benzoxazol-2-alicyclic amide derivatives were synthesized by the reaction of the N-alicyclic secondary amine analogs with the intermediates obtained from the reaction of 2-aminophenol derivatives and diethyl oxalate. This study used diethyl oxalate as a starting material to react with 2-aminophenol derivatives (**1–5**). Under reflux conditions, substituted 2-aminophenols (**1–5**) underwent a substitution reaction with diethyl oxalate (**6**), affording the corresponding amino-oxo-acetate intermediates (**7–11**) with 70%–95% yields. The intermediates were cyclized with triphenylphosphine (PPh_3; **12**) and diethylazodicarboxylate (DEAD; **13**) to obtain benzoxazole-2-ethyl-carboxylates (**14–18**) with 50%–90% yields. The amidation of compounds **14–18** was carried out using pyrrolidine, piperidine, 4-methylpiperidine, and morpholine in the presence of tetrahydrofuran (THF) to afford the benzoxazole alicyclic amide derivatives, which were the corresponding final products (**B1–B20**) in 56%–98% yields. The proposed structures of the compounds agreed with the ^1H NMR, ^{13}C NMR, and elemental analyses.

3.2. Biological Activity Studies

For many reasons, including drug toxicity and side effects, a more comprehensive investigation of different signaling pathways is required to identify new targets for cancer treatment. The PI3K/Akt/mTOR signalling pathway is active in many diseases such as breast and ovarian cancer. While this pathway is necessary for growth, proliferation and cell survival in normal cells, it is an undesirable feature in cancer cells. The PI3K/Akt/mTOR signalling pathway interacts with AMP-activated protein kinase (AMPK), Wnt/β-catenin, mitogen-activated protein kinase (MAPK) and other intracellular signaling pathways. Investigating the potential effects of newly developed anticancer drugs on these pathways can be useful in understanding the target of cancer treatment. In vitro determination of mTOR inhibitory activity.

3.2.1. MTT

In the activity studies, the cytotoxic effects of the synthesized chemical compounds on MCF-7 cell line at 48 and 78 h were investigated (Table 1). IC_{50} values of the synthesized chemical compounds were calculated. In vitro mTOR inhibitory activity determination studies, in which the lowest IC_{50} value was calculated 48 and 72 h after the application, continued with compounds B4, B11, B12, and B20, which were determined to be active.

3.2.2. Evaluation of mTOR Kinase Inhibitory Activities of the Compounds In Vitro MCF-7 Cell Lines

In order to evaluate the inhibitory effect of the compounds B4, B11, B12, and B20 on mTOR kinase, we measured the level of phosphorylated mTOR Ser2448 in treated MCF-7 cells (48 h). The results illustrated in Figure 6 that the compounds B12 and B20 showed significant inhibitory effect on phosphorylation of mTOR at Ser2448 compared to control.

The results showed that B12 and B20 decreased the increased p-mTOR (Ser2448)/mTOR ratio in MCF-7 cells, whereas B4 and B11 did not significantly decrease this ratio. The mTOR inhibitor rapamycin, which we used as a positive control, also decreased

© 2025 Wiley-VCH GmbH

23656549, 2025, 21, Downloaded from https://chemistry-europe.onlinelibrary.wiley.com/doi/10.1002/slct.202501424 by Erzincan Universitesi, Wiley Online Library on [01/06/2025]. See the Terms and Conditions (https://onlinelibrary.wiley.com/terms-and-conditions) on Wiley Online Library for rules of use; OA articles are governed by the applicable Creative Commons License

Table 1. IC_{50} values of 20 synthesized chemical compounds calculated 48 and 72 h after MTT application.

Compounds	IC_{50} (μM)	
	(48 h)	(72 h)
B1	19,84	15,80
B2	28,78	23,50
B3	23,04	20,16
B4	10,84	8,75
B5	21,99	19,84
B6	38,50	37,62
B7	40,36	38,59
B8	36,63	33,77
B9	40,06	35,50
B10	41,85	37,73
B11	6,40	5,83
B12	6,82	4,96
B13	32,59	30,72
B14	21,71	19,53
B15	41,00	38,54
B16	12,49	10,25
B17	31,17	28,67
B18	39,18	37,93
B19	39,09	38,45
B20	11,57	9,82

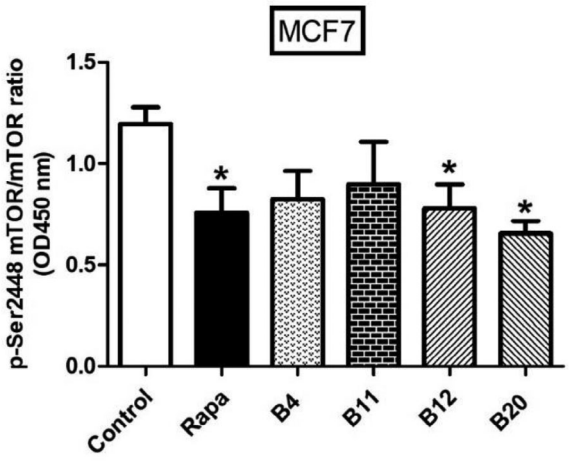

Figure 6. Effects of the compounds on the phosphorylation of mTOR at the Ser2448 position in the MCF-7 cell line. Phosphorylation of mTOR at the Ser2448 position is shown as the ratio of OD values at 450 nm as mean ±SEM ($n = 6$). RAPA, rapamycin. * Statistically significant difference from control group values (Student's t test; $p < 0.05$). MCF-7 cells were incubated with 0.1% DMSO (control), B4, B11, B12, B20, and rapamycin for 48 h.

the increased mTOR activity in MCF-7 cells as shown in Figure 6. According to our findings, it was shown for the first time in this study that the newly synthesized compounds B12 and B20 may have inhibitory activity on the increased mTOR activity in MCF-7 breast cancer cells.

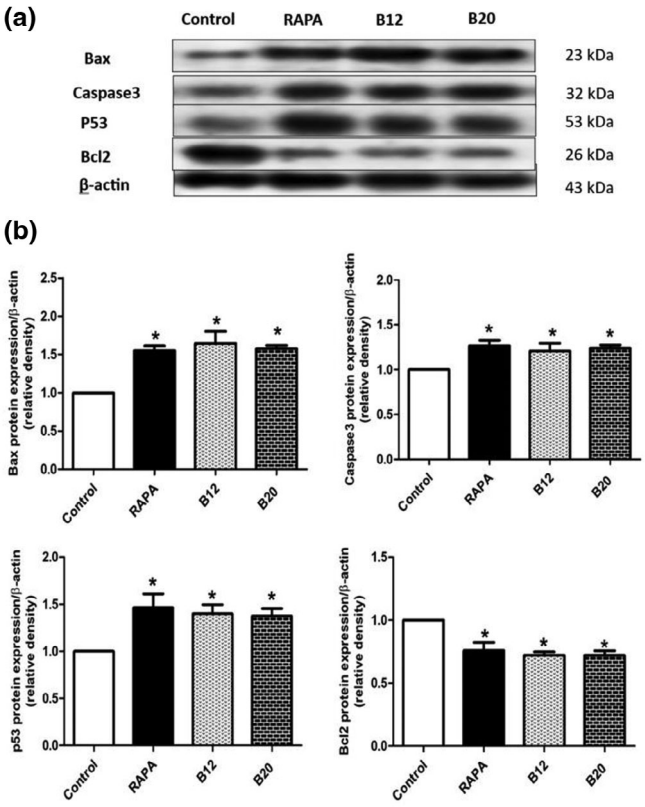

Figure 7. Effects of B12 and B20 on the expression of proapoptotic and antiapoptotic proteins Bax, caspase-3, p53, and Bcl2 in the MCF-7 breast cancer cell line. (a) Representative immunoblot band images of pro-apoptotic and anti-apoptotic proteins, (b) quantitative analysis of the expressions of relevant proteins. Results are presented as mean ±SEM ($n = 4$). RAPA, rapamycin. * Statistically significantly different from control group values (Student's t test; $p < 0.05$).

3.2.3. The Effect of the Compounds B12 and B20 on the Expression of Bax, Caspase3, p53, and Bcl2 Proteins

To assess whether compounds B12 and B20 would induce cell apoptosis, we examined the expression of Bax, caspase3, p53, and Bcl2 as the proapoptotic or antiapoptotic markers in B12 and B20 treated MCF-7 cells (48 h) by immunoblot assay. The results were illustrated in Figure 7. that compounds B12 and B20 increased the expression of Bax, caspase3, and p53 proteins that are proapoptotic markers while showed inhibitory effect of the expression of antiapoptotic Bcl2 protein compared to control.

3.3. In Silico Studies

3.3.1. Molecular Docking

Within the scope of in silico studies, molecular modeling studies were performed on compounds B4, B11, B12, and B20, which have the best IC_{5n} values as a result of MTT analyses. The mTOR (4JT5) structure, which regulates cell growth, metabolism, and proliferation, was selected as the target protein. This structure is of enormous importance in terms of understanding the ATP binding site of mTOR and the inhibitor binding mechanism. Within

© 2025 Wiley-VCH GmbH

23656549, 2025, 21, Downloaded from https://chemistry-europe.onlinelibrary.wiley.com/doi/10.1002/slct.202501424 by Erzincan Universitesi, Wiley Online Library on [01/06/2025]. See the Terms and Conditions (https://onlinelibrary.wiley.com/terms-and-conditions) on Wiley Online Library for rules of use; OA articles are governed by the applicable Creative Commons License

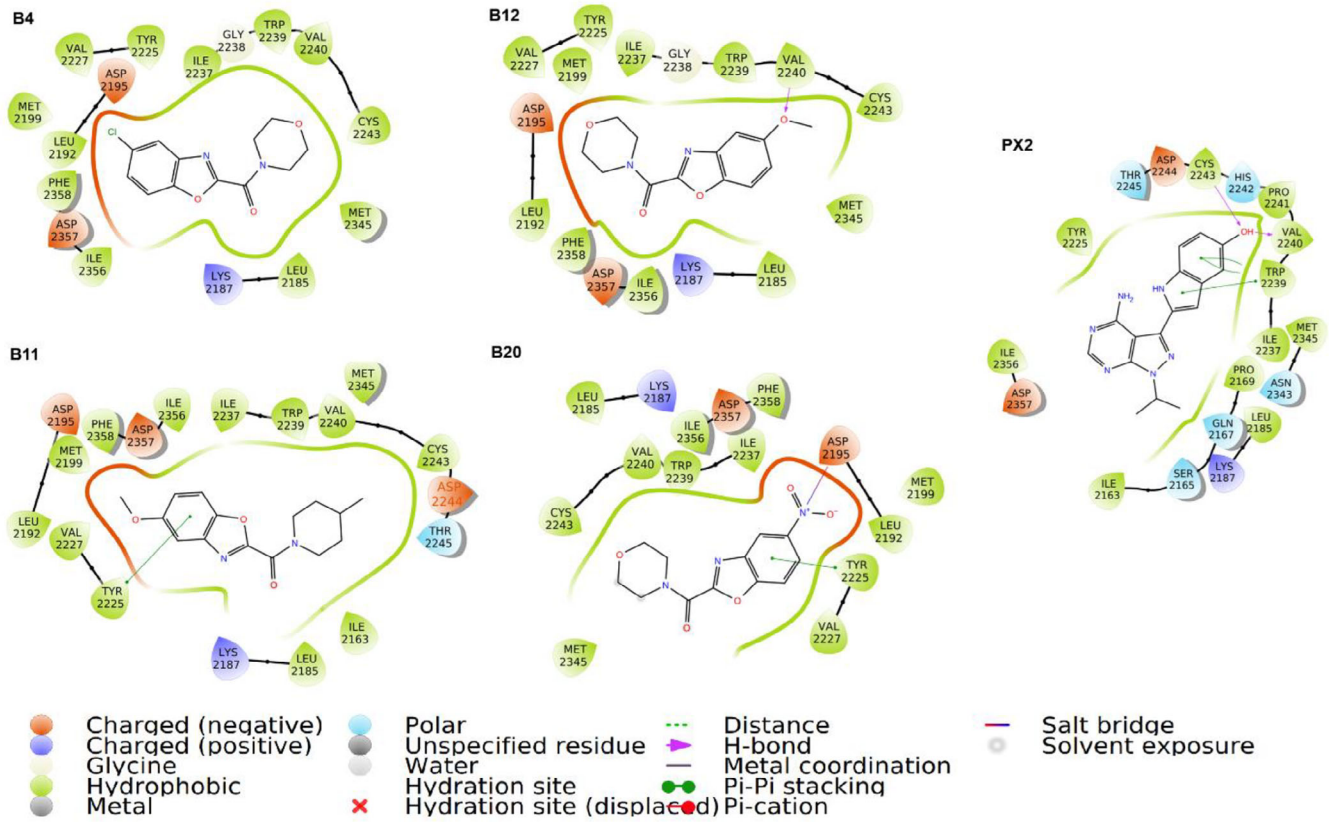

Figure 8. 2D interaction of B4, B11, B12, B20, and P2X with residues in the active site of 4JT5.

Table 2. Docking and MM-GBSA scores of B4, B11, B12, and B20 (kcal/mol).

Compounds	Molecular Docking	MM-GBSA
B4	−7.084	−43.90
B11	−7.220	−43.13
B12	−7.426	−42.69
B20	−7.113	−44.80
P2X	−7.309	−39.55

the scope of molecular modeling studies, the interactions of the compounds with the residues in the active site of 4JT5 were examined in detail (Figure 8). In addition, the docking scores and MM-GBSA (kcal/mol) scores of the compounds were calculated and evaluated (Table 2).

In molecular modeling studies, P2X, which is found in the 4JT5 structure, was used as the reference compound. P2X is a second-generation, ATP-competitive mTOR inhibitor, and it suppresses mTOR activity by interacting with the ATP binding site of mTOR. While the docking score of P2X was determined as −7.309 kcal/mol, the docking scores of the tested compounds were calculated in the range of−7.084 to −7.426 kcal/mol. The obtained data show that the docking scores of the compounds are quite close to P2X (Table 2). In the literature,[1,2] Asp2195, Lys2187, Val2240, Trp2239, and Asp2357 residues have been reported to be critical for the 4JT5 (mTOR) protein. As a result of the analysis, it was determined that compounds B20, B12, B11, and B4 formed hydrophobic interactions with Cys2243, Val2240, Trp2239, Ile2237, Tyr2225, Met2199, Val2227, Leu2192, Phe2358, Ile2356, Leu2185, and Met2345 residues. The compounds also exhibited negatively charged interactions with Asp2195 and Asp2357 and positively charged interactions with Lys2187. Unlike other compounds, compound B12 formed a hydrogen bond with Val2240, while the reference compound P2X formed a hydrogen bond with Cys2243 and Val2240 and a $\pi-\pi$ stacking interaction with Trp2239. In addition, P2X was observed to exhibit a negatively charged interaction with Lys2187 and to form additional polar interactions such as Gln2167, Ser2165, and Asn2343, unlike the synthesized compounds.

It was determined that compounds B20, B12, B11, and B4 bind to the active site of the 4JT5 (mTOR) protein and exhibit a similar interaction profile to P2X. It is thought that these compounds contribute to mTOR inhibition by interacting with critical residues such as Asp2195, Lys2187, Trp2239, and Val2240. Structural analyses show that the benzoxazole ring contributes to the binding mechanism by interacting with hydrophobic residues similar to the indole ring found in P2X.

In general, the obtained data suggest that compounds B20, B12, B11, and B4 can be considered as potential candidates in mTOR inhibition.

3.3.2. Molecular Dynamics (MD) Simulation Studies

In MD simulation studies, compounds B12 and B20, which have the highest inhibition value against mTOR, were analyzed. As a

© 2025 Wiley-VCH GmbH

23656549, 2025, 21, Downloaded from https://chemistry-europe.onlinelibrary.wiley.com/doi/10.1002/slct.202501424 by Erzincan Universitesi, Wiley Online Library on [01/06/2025]. See the Terms and Conditions (https://onlinelibrary.wiley.com/terms-and-conditions) on Wiley Online Library for rules of use; OA articles are governed by the applicable Creative Commons License

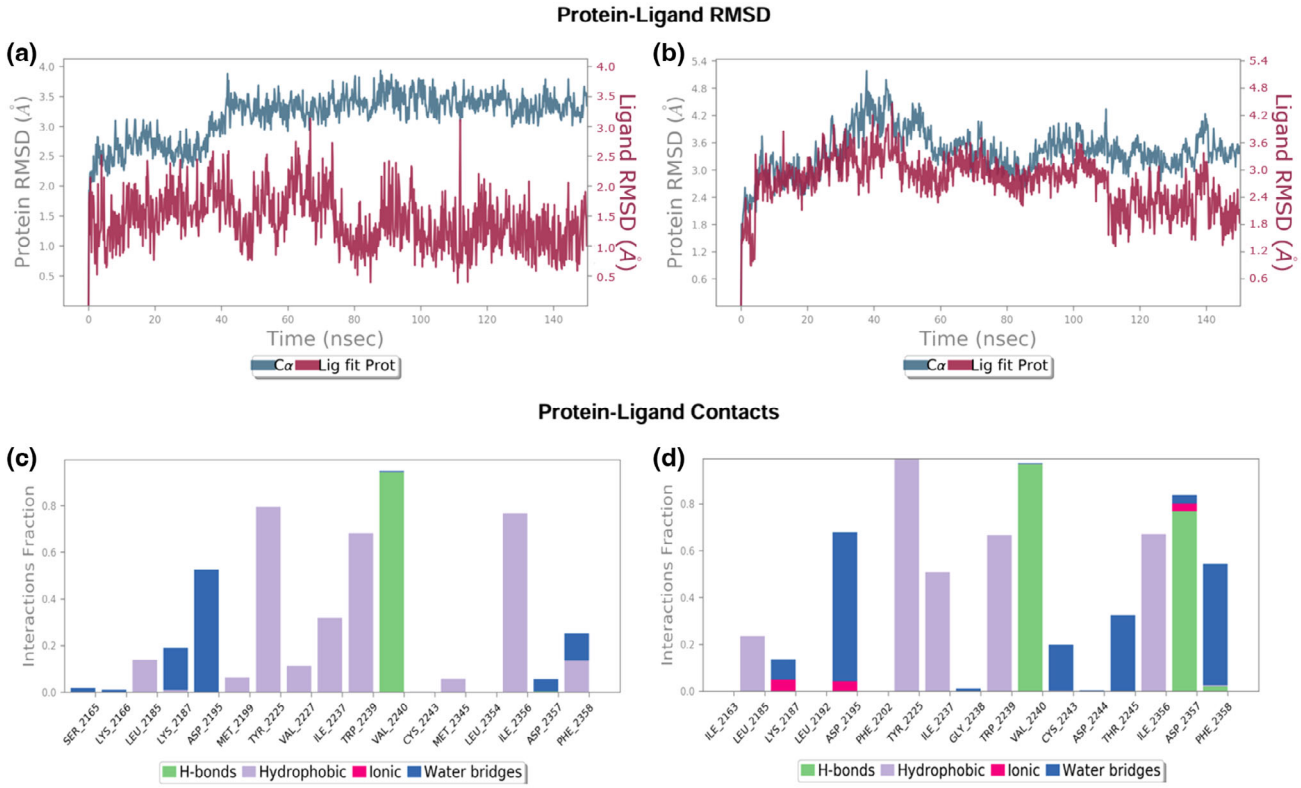

Figure 9. RMSD (Root Mean Square Deviation) change graphs of compounds (a) B12 and (b) B20 in 4JT5 protein during MD simulations performed for 150 ns. Fractional distribution of residue-based interactions of compounds (c) B12 and (d) B20 during MD simulations.

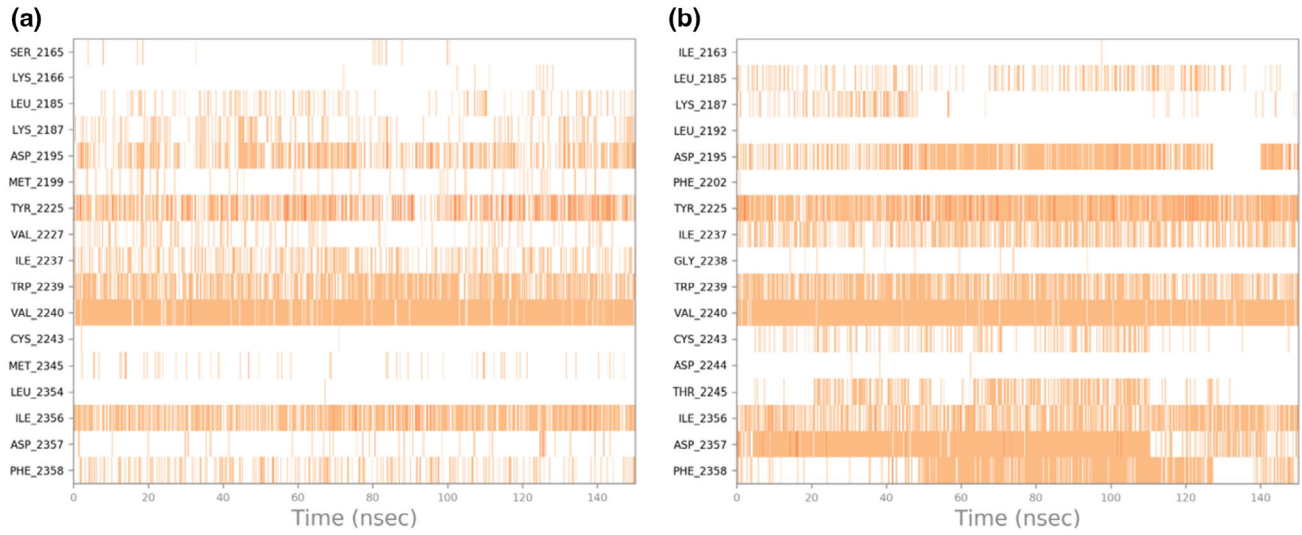

Figure 10. Specific interactions of compounds (a) B12 and (b) B20 with the protein during MD simulations (contact points obtained along the trajectory).

result of docking studies of B20 and B12, the best binding positions were determined, and MD simulations were conducted for 150 ns based on this structure. The RMSD value of B12 varied between 0.5 Å and 3.3 Å from the beginning of the simulation for 150 ns (Figure 9a). B12 continues to contact Asp2195, Tyr2225, Ile2237, and Ile2356 for 150 ns. In addition, B12 maintained its interaction with Trp2239 and Val2240, which are critical for the 4JT5 protein, throughout the simulation period (Figure 10a). B12 formed hydrogen bonds with Val2240 during almost the entire simulation period. The compound exhibited hydrophobic interactions with Tyr2225 (80%), Ile2356 (76), Trp2239 (69%), and Ile2356 (55%) for a significant portion of the simulation period (Figure 9c).

In the simulation studies performed for the B20 compound, which has the highest inhibition value against mTOR, the protein RMSD value varied between 1.2 Å and 4.2 Å. The ligand RMSD value remained stable between 0 and 150 ns, and its average value was calculated as approximately 3 Å. (Figure 9b). When the

© 2025 Wiley-VCH GmbH

23656549, 2025, 21, Downloaded from https://chemistry-europe.onlinelibrary.wiley.com/doi/10.1002/slct.202501424 by Erzincan Universitesi, Wiley Online Library on [01/06/2025]. See the Terms and Conditions (https://onlinelibrary.wiley.com/terms-and-conditions) on Wiley Online Library for rules of use; OA articles are governed by the applicable Creative Commons License

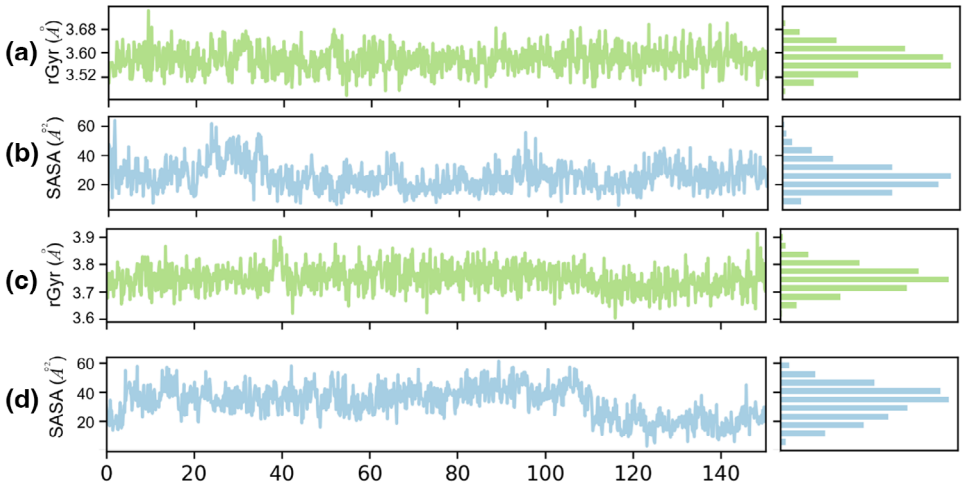

Figure 11. Radius of gyration (rGyr) and solvent accessible surface area (SASA) analysis of the B12 and B20 during the 150 ns MD simulation. (a,b) B12 in 4JT5 and (c,d) B20 in 4JT5.

specific contacts between the protein and ligand were examined throughout the simulation, it was observed that B20 lost its interaction with Lys2187 after 50 ns. B20 maintained interactions with Asp2195, Tyr2225, Ile2237, Tyr2239, Val2240, and Ile2356 throughout the simulation period, similar to B12. (Figure 10b). B20 established hydrophobic interactions with Tyr2225 (throughout the entire period), Trp2239 (for 60%), and Ile2356 (for 20%) of the simulation time (Figure 9d).

Radius of Gyration (rGyr) is an important MD simulation parameter that evaluates the structural compactness and stability of a molecule over time. In simulation studies, the effect of the complexes formed by the B12 and B20 with mTOR on rGyr was investigated (Figure 11). The rGyr value of B12 varies between 3.52 Å and 3.68 Å over 150 ns (Figure 10a), while the value of B20 varies between 3.60 Å and 3.90 Å (Figure 10c). The rGyr changes of B12 and B20 are 4.54% and 8.33%, respectively.

Another important MD simulation parameter that explains the stability of ligand-protein complexes is the solvent accessible surface area (SASA) analysis. SASA analysis describes the stability of ligand-protein complexes by evaluating the surface area of molecules in water. The SASA values of B12 (Figure 10b) and B20 (Figure 10d) are approximately between 20 and 60 Å^2. rGyr and SASA analyses support that B12 and B20 remain in stable conformations within the protein.

3.3.3. ADMET Analysis

Many compounds, although biologically active, cannot be used as drugs due to their negative ADMET (properties, drug-likeness, and estimated toxicity) properties. In our study, the ADMET properties of the compounds were evaluated in silico (Table 3). The QPPCaco value indicates the absorption status of the compounds in the small intestine. QPPCaco values of B4, B11, and B12 (2501.77, 2941.47, and 2601.56) indicate that their absorption from the small intestine is quite high. The absorption of B20 is low compared to other compounds. The human oral absorption percentages for B4, B11, and B12 are quite high. These values indicate that the compounds can be used orally. The metab values of the compounds are within the recommended range (1–8), signifying their metabolic stability. All compounds exhibit LogP and QPlogBB values within the recommended range. These values indicate that the compounds' absorption and bioavailability enable them to traverse the blood-brain barrier. The drug potential of the compounds was evaluated according to the Rule of Five, Rule of Three, Veber, Egan, Ghose, and Muegge rules. All of the compounds comply with these rules. QPlogHERG values of the compounds associated with cardiac toxicity were found to be within the recommended range. In silico studies determined that the compounds did not have any predicted toxic properties (mutagenic, tumorogenic, or irritant).

4. Conclusion

Cytotoxicity study was performed with benzoxazole derivatives which had the highest inhibition value against mTOR. In vitro activity of the compounds was performed by MTT assay against MCF-7 cell line. Compounds B4, B11, B12, and B20 showed the best IC_{50} value against MCF-7. These results provided an important basis for further optimization of compounds B4, B11, B12, and B20 as a potential anticancer agent.

Based on the data obtained from cytotoxicity studies, biological activity studies were performed with compounds B4, B11, B12, and B20. These studies revealed that compounds B12 and B20 demonstrated significant mTOR kinase inhibitory activity. Furthermore, we deduced from the design of this study that B12 and B20, which showed strong mTOR inhibition, also possess substantial apoptotic potential. It is evident from the trend benzoxazole is a significant therapeutic scaffold that enable the development of target-based agents for the treatment of various cancer types. As mTOR targeted derivatives, mTOR kinase-inhibiting benzoxazole derivatives could be helpful in the creation of long-term, promising anticancer medication options. Continuous research and clinical evaluations should be carried out to further develop benzoxazole derivatives with therapeutic potential.

© 2025 Wiley-VCH GmbH

23656549, 2025, 21, Downloaded from https://chemistry-europe.onlinelibrary.wiley.com/doi/10.1002/slct.202501424 by Erzincan Universitesi, Wiley Online Library on [01/06/2025]. See the Terms and Conditions (https://onlinelibrary.wiley.com/terms-and-conditions) on Wiley Online Library for rules of use; OA articles are governed by the applicable Creative Commons License

23656549, 2025, 21, Downloaded from https://chemistry-europe.onlinelibrary.wiley.com/doi/10.1002/slct.202501424 by Erzincan Universitesi, Wiley Online Library on [01/06/2025]. See the Terms and Conditions (https://onlinelibrary.wiley.com/terms-and-conditions) on Wiley Online Library for rules of use; OA articles are governed by the applicable Creative Commons License

Table 3. ADME, drug-likeness, and toxic properties of compounds.

	B4	B11	B12	B20
ADME				
MW	266,68	274,31	262,26	277,23
LogP	1100	2141	0706	−0120
QPPCaco	2501,77	2941,47	2601,56	316,23
QPlogBB	0147	−0052	−0076	−0900
PSA	60943	59419	68442	104674
#Metab	2	2	3	3
QPlogKhsa	−0953	−0392	−1101	−1181
% Human Oral Abs.	94206	100,00	92204	70989
CYP450 inhibition	1A2,2C19	1A2, 2C19 2C9, 2D6	1A2	1A2
Drug-likeness				
Rule of Five	0	0	0	0
Rule of Three	0	0	0	0
Veber	Yes	Yes	Yes	Yes
Egan	Yes	Yes	Yes	Yes
Ghose	Yes	Yes	Yes	Yes
Muegge	Yes	Yes	Yes	Yes
Toxicity				
Mutagenic	No	No	No	No
Tumorogenic	No	No	No	No
Irritant	No	No	No	No
QPlogHERG	−3974	−4354	−4021	−4026

LogP: Predicted octanol/water partition coefficient (−2.0–6.5). **QPPCaco**: Predicted apparent Caco-2 cell permeability in nm/sec. Caco-2 cells are a model for the gut-blood barrier. QikProp predictions are for non-active transport (<25 poor, >500 great). **QPlogBB**: Predicted brain/blood partition coefficient (−3.0–1.2). **#metab**: Number of likely metabolic reactions (1–8). **QPlogKhsa**: Prediction of binding to human serum albümin (−1.5–1.5). **% Human Oral Absorption**: Predicted human oral absorption on 0 to 100% scale (>80% is high <25% is poor). **PSA**: Van der Waals surface area of polar nitrogen and oxygen atoms and carbonyl carbon atoms (7.0–200.0). **Rule Of Five**: Number of violations of Lipinski's rule of five (maximum is 4). **Rule Of Three**: Number of violations of Jorgensen's rule of three (maximum is 3). **QPlogHERG**: Predicted IC50 value for blockage of HERG (concern below −5).

Structure–activity relationship (SAR) analysis of the synthesized compounds revealed that four different core scaffolds and five distinct substituents were explored. It was observed that compounds containing pyrrolidine and piperidine rings generally did not exhibit cytotoxic activity, regardless of the substituents. In contrast, morpholine-containing derivatives showed significant activity, particularly those substituted with chloro and nitro groups. Additionally, 4-methylpiperidine derivatives exhibited activity only in the presence of methoxy substituents. These findings suggest that while no single substituent emerged as a universal determinant of activity, the presence of the morpholine ring appears to contribute substantially to cytotoxic efficacy. Evaluation of mTOR kinase inhibitory activities using MCF-7 cell lines highlighted the notable activity of compounds B12 and B20, both of which contain a morpholine moiety. Although this ring system was not found to play a prominent role in molecular docking interactions, it is hypothesized that the total electronic distribution conferred by the morpholine ring may enhance the overall interaction of the molecule with the active site of mTOR.

MD simulation studies were also conducted with B12 and B20, the most active compounds against mTOR. According to the simulation results, both compounds remained stable in the active site of the protein, suggesting their potential as mTOR inhibitors. In silico ADMET analysis indicated that the pharmacokinetic and toxicity profiles of these compounds were within acceptable ranges, further supporting their potential for further development.

Acknowledgements

This work was financially supported by Inönü University-Research Project of TCD-2021–2368. The authors would also like to thank Mersin University Advanced Technology Education, Research and Application Center (MEITAM) for their valuable assistance and Erzincan Binali Yıldırım University Research Fund (Project no: TCD-2025–1019).

Conflict of Interests

The authors declare no conflict of interest.

© 2025 Wiley-VCH GmbH

Author Contributions

Mehmet Abdullah Alagoz, Meryem Temiz Resitoglu, Derya Yetkin, Rukiye Nalan Tiftik, Seyhan Sahan Firat, and Oztekin Algul conceived and designed the experiments. Mehmet Abdullah Alagoz, Meryem Temiz Resitoglu, Burak Kuzu, Zainab Sabrie, Derya Yetkin, Cengiz Zobi, Rukiye Nalan Tiftik performed the experiments. Mehmet Abdullah Alagoz, Meryem Temiz Resitoglu, Derya Yetkin, Rukiye Nalan Tiftik, Sule Gursoy, Ceylan Hepokur, Seyhan Sahan Firat, and Oztekin Algul analyzed the data. Mehmet Abdullah Alagoz, Meryem Temiz Resitoglu, Seyhan Sahan Firat, and Oztekin Algul wrote the paper.

Data Availability Statement

Research data are not shared.

Keywords: Apoptotic effect · Benzoxazole · Molecular docking · MTOR · Structure–activity relationship

[1] A. F. Ajayi, M. O. Oyovwi, O. P. Akano, G. B. Akanbi, F. B. Adisa, *Cancer Cell Int.* **2025**, *25*, 33.
[2] N. Shaharudin, G. Surindar Singh, T. L. Kek, S. Sultan, *Mol. Clin. Oncol.* **2024**, *21*, 81.
[3] C. Glorieux, C. Enríquez, P. Calderon, *Biochem. Pharmacol.* **2025**, *232*, 116729.
[4] S. H. Hare, A. J. Harvey, *Am. J. Cancer Res.* **2017**, *7*, 383.
[5] J. Huan, P. Grivas, J. Birch, D. E. Hansel, *Cancers* **2022**, *14*, 1555.
[6] M. Ali, S. A. Bukhari, H. W. Lee, *BMB Rep.* **2017**, *50*, 601.
[7] S. Huang, *Cells* **2020**, *9*, 2278.
[8] M. Cargnello, J. Tcherkezian, P. P. Roux, *Mutagenesis* **2015**, *30*, 169–176.
[9] C. Magaway, E. Kim, E. Jacinto, *Cells* **2019**, *8*, 1584.
[10] B. Mao, Q. Zhang, L. Ma, D. S. Zhao, P. Zhao, P. Yan, *Molecules* **2022**, *27*, 5295.
[11] Y. Chen, X. Zhou, *Eur. J. Med. Chem.* **2020**, *208*, 112820.
[12] E. S. Ali, K. Mitra, S. Akter, S. Ramproshad, B. Mondal, I. N. Khan, M. T. Islam, J. S. Rad, D. Calina, W. C. Cho, *Cancer Cell Int.* **2022**, *22*, 284.
[13] Z. Lu, X. Shi, F. Gong, S. Li, Y. Wang, Y. Ren, M. Zhang, B. Yu, Y. Li, W. Zhao, J. Zhang, G. Hou, *Acta Pharm. Sin. B* **2020**, *10*, 1004–1019.
[14] Z. Lu, Y. Zhang, Y. Xu, H. Wei, W. Zhao, P. Wang, Y. Li, G. Hou, *Mol. Biol. Rep.* **2022**, *49*, 451–461.
[15] M. Zeng, Y. Hu, L. Zhao, C. Duan, H. Wu, Y. Xu, X. Liu, Y. Wang, D. Jiang, S. Zeng, *Eur. J. Med. Chem.* **2025**, *284*, 117200.
[16] X. K. Wong, K. Y. Yeong, *ChemMedChem* **2021**, *16*, 3237–3262.
[17] J. Lou, J. X. Lv, Y. P. Zhang, Z. J. Liu, *Cell Biol. Int.* **2022**, *46*, 1204–1214.
[18] N. Lin, L. Sun, J. Chai, H. Qi, Y. Zhao, J. Ma, M. Xia, X. Hu, *Cancer Cell Int.* **2024**, *24*, 38.
[19] G. Angajala, R. Subashini, *Struct. Chem.* **2020**, *31*, 263–273.
[20] W. Zhong, X. Tang, Y. Liu, C. Zhou, P. Liu, E. Li, P. Zhong, H. Lv, Q. Zou, M. Wang, *Molecules* **2020**, *25*, 971.
[21] A. Podolski-Renić, Z. Milošević, J. Dinić, T. Stanković, J. Banković, M. Pešić, *MedChemComm* **2016**, *7*, 2265–2281.
[22] A. P. Pinto, A. L. da Rocha, B. B. Marafon, J. E. Nogueira, L. G. Branco, J. R. Pauli, L. P. de Moura, D. E. Cintra, E. R. Ropelle, A. S. da Silva, *Clin. Exp. Pharmacol. Physiol.* **2022**, *49*, 893–902.
[23] İ. Çapan, M. Hawash, M. T. Qaoud, L. Gülüm, E. N. Y. Tunoglu, K. U. Çifci, B. S. Çevrimli, Y. Sert, S. Servi, İ. Koca, Y. Tutar, *BMC Chem.* **2024**, *18*, 102.
[24] J. Li, J. Han, Y. Shi, M. Liu, *Exp. Eye Res.* **2023**, *233*, 109539.
[25] X. Zhu, Q. Liu, M. Wang, M. Liang, X. Yang, X. Xu, H. Zou, J. Qiu, *PLoS One* **2011**, *6*, e27081.
[26] V. S. Ionescu, A. Popa, A. Alexandru, E. Manole, M. Neagu, S. Pop, *Antioxidants* **2021**, *10*, 1893.
[27] C. F. Wu, Q. C. Wang, R. Chen, H. L. Zhou, T. T. Wu, Y. Du, N. N. Zhang, H. M. Zhang, Z. Y. Fan, L. L. Wang, C. J. Hu, Z. P. Sang, H. L. Li, L. Wang, L. Tang, J. Q. Zhang, *Eur. J. Med. Chem.* **2022**, *229*, 114055.
[28] A. H. Tantawy, M. F. El-Behairy, W. H. Abdallah, H. Jiang, M. Q. Wang, A. A. Marzouk, *J. Med. Chem.* **2021**, *64*, 17468–17485.
[29] Q. Sun, Y. Chu, N. Zhang, R. Chen, L. Wang, J. Wu, Y. Donk, H. Li, Li, W., L. Tang, C. Zhan, J. Q. Zhang, *J. Med. Chem.* **2024**, *67*, 7330–7358.
[30] Y. Hou, F. Zhang, W. Min, K. Yuan, W. Kuang, X. Wang, Y. Zhu, C. Sun, F. Xia, Y. Wang, H. Zang, L. Wang, P. Yang, *J. Med. Chem.* **2022**, *65*, 9873–9892.
[31] S. Park, Y. S. Kim, D. Y. Kim, I. So, J. H. Jeon, *Biochim. Biophys. Acta (BBA)-Rev. Cancer* **2018**, *1870*, 198–206.
[32] B. Kuzu, F. Ayaz, O. Aigul, *J. Heterocycl. Chem.* **2019**, *56*, 1946–1952.
[33] B. Kuzu, C. Hepokur, *Bioorg. Med. Chem. Rep.* **2020**, *3*, 15-21.
[34] B. Kuzu, C. Hepokur, O. Algul, *Org. Commun.* **2023**, *16*, 3.
[35] B. Kuzu, O. Sari, S. S. Erdem, O. Algul, N. Menges, *ChemistrySelect* **2021**, *6*, 2529–2538.
[36] B. Kuzu, C. Hepokur, M. A. Alagoz, S. Burmaoglu, O. Algul, *ChemistrySelect* **2022**, *7*, e202103559.
[37] Y. Zhu, A. Wang, S. Zhang, J. Kim, J. Xia, F. Zhang, D. Wang, Q. Wang, J. Wang, *J. Adv. Res.* **2023**, *49*, 159–173.
[38] A. Sain, T. Kandasamy, D. Naskar, *J. Biomol. Struct. Dyn.* **2022**, *40*, 10962–10977.
[39] H. Şenol, M. Ghaffari-Moghaddam, Ş. Bulut, F. Akbaş, A. Köse, G. Topçu, *Chem. Biodivers.* **2023**, *20*, e202301089.
[40] X. Luo, J. Wang, R. Wang, J. Lian, M. Guo, H. Zhou, M. Zhang, Z. Yang, X. Li, X. He, X. Bi, *RSC Med. Chem.* **2024**, *15*, 3460–3468.
[41] B. Kuzu, M. A. Alagoz, Y. Demir, I. Gulcin, S. Burmaoglu, O. Algul, *Mol. Divers.* **2024** *29*, 671–693.
[42] B. O. Aydin, D. A. Anil, Y. Demir, M. A. Alagoz, *Mol. Divers.* **2024**, *28*, 3739–3755.

Manuscript received: March 10, 2025

© 2025 Wiley-VCH GmbH

23656549, 2025, 21, Downloaded from https://chemistry-europe.onlinelibrary.wiley.com/doi/10.1002/slct.202501424 by Erzincan Universitesi, Wiley Online Library on [01/06/2025]. See the Terms and Conditions (https://onlinelibrary.wiley.com/terms-and-conditions) on Wiley Online Library for rules of use; OA articles are governed by the applicable Creative Commons License